Characterization of Vesicles Formed by Alkenesuccinic Acids

KAZUMA NAKAZAWA AND TOYOKO IMAE[1]

Department of Chemistry, Faculty of Science, Nagoya University, Nagoya 464, Japan

Received July 12, 1991; accepted November 26, 1991

Differential thermal analysis (DTA), electron spin resonance (ESR), and gel filtration were carried out for vesicle solutions of alkenesuccinic acids (C_nSA). The gel–liquid crystal phase transitions were confirmed by DTA. It was certified by a spin probe ESR method that the ordering of molecular motion in a vesicle changed remarkably at temperatures above and below the metagel–liquid crystal phase transition. The trapping efficiency of anionic dye was evaluated from gel filtration. The percolation of dye from the inner aqueous phase in a vesicle increased remarkably above the phase transition temperature, being related to the disordering of vesicle bilayers.

INTRODUCTION

It can be observed by differential scanning calorimetry (DSC) that the gel–liquid crystal phase transition occurs in turbid solutions of native and synthetic amphiphiles (1, 2). The phase transition is attributed to the trans–gauche configurational transition in hydrocarbon chain moiety of amphiphiles so that the flexibility of hydrocarbon chains or the fluidity of bilayer membranes changes and, therefore, the membrane permeability of small substances such as sugar increases above the phase transition temperature (3).

The variation of local environment in the bilayer membranes accompanied with the phase transition can be clarified by measuring the motion of probe molecules that are embedded in the bilayers. Fluorescence spectroscopy (4) and electron spin resonance (ESR) (5) are often used for this purpose.

In the ESR measurement, spin-labeled fatty acids, *n*-DOXYL stearic acids, are generally utilized as probe molecules. These spin probes have a *N*-oxyloxazolidine ring retaining a nitroxide radical on a hydrocarbon chain of stearic acid. If the hyperfine splits are measured at various temperatures on the ESR spectra of spin labels in bilayer membranes, the temperature dependence of the degree of order of hydrocarbon chains in the bilayers can be evaluated (5).

Satoh and Tsujii (6) have reported that 1–2 wt% aqueous solutions of hexadecenesuccinic acid (C_{16}SA) presented spontaneously iridescent color at high temperatures. They suggested that lamellar layers formed in those solutions and clarified the relation with the phase transition from DSC measurement. Imae and Trend (7) have observed vesicle-like particles with membrane layers in iridescent C_{16}SA solutions by means of video-enhanced differential interference contrast microscopy (VEM). Similar but smaller vesicles with membrane structures were certified by VEM (8) and transmission electron microscopy (9) in dilute, aqueous solutions of potassium alkenesuccinates (C_nSAK) and alkenesuccinic acids (C_nSA) at medium pH and room temperature.

Although these facts suggest that vesicle formation occurs in aqueous solutions of single-chain amphiphiles, C_nSAK and C_nSA, and is dependent on temperature and pH, the characteristics of vesicles such as the motional state of bilayers and the existence of inner aqueous phases are not yet known. The aim of the present study is to clarify such charac-

[1] To whom correspondence should be addressed.

0021-9797/92 $5.00

teristics as functions of hydrocarbon chain length of C_nSA, solution concentration, temperature, and medium pH, which are investigated by differential thermal analysis (DTA), ESR, and gel filtration for vesicle solutions of C_nSA.

EXPERIMENTAL

Materials

Alkenesuccinic acids (C_nSA, n = 14, 16; $CH_3(CH_2)_{n-4}CH{=}CHCH_2CH(COOH)$-$CH_2COOH$) and disodium dodecenesuccinic acid ($C_{12}SANa$) are identical to samples previously prepared and used (10). $C_{12}SA$ was precipitated by adding HCl to $C_{12}SANa$ in water and recrystallized from acetone. *n*-DOXYL stearic acids (n = 5, 7, 12, 16) were purchased from Aldrich.

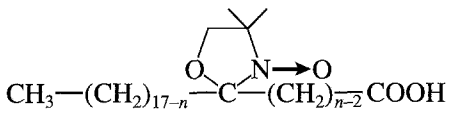

Water was redistilled from alkaline $KMnO_4$ and degassed by sonicating for 30 min under reduced pressure by an aspirator. A standardized HCl solution, chloroform, and bromophenol blue are commercial products. Methanol was distilled. Phosphate buffer solutions were prepared by dissolving commercial $NaH_2PO_4 \cdot 2H_2O$ and $Na_2HPO_4 \cdot 10H_2O$ in water and mixing them at an appropriate ratio for a desired pH.

Differential Thermal Analysis (DTA)

C_nSA was dissolved in 1/15 M phosphate buffer or in water by heating. Solution pH was measured on an Iwaki Glass pH/ion meter M-225 under nitrogen atmosphere. The solution in a DTA test tube was kept overnight at 5°C, resulting in the precipitates. A test tube equipped with a DTA heating block was successively heated, cooled, and reheated. The rates of heating and cooling processes were about 7 and 3°C min^{-1}, respectively. The C_nSA solution in the tube was visually observed at the temperatures above and below the phase transition. A cupper-constantan thermocouple was used, and the melting temperature of ice was adopted as a standard temperature. Al_2O_3 was utilized as a reference. The DTA apparatus is a noncommercial product designed by Professors D. Nakamura and R. Ikeda's group at Nagoya University.

Electron Spin Resonance

The spin-labeled reagent, *n*-DOXYL stearic acid, in methanol was mixed at the concentration of 1 mol% with C_nSA in methanol: chloroform (2:1 by volume). After the solvents were evaporated, the residual thin film was dried for more than 2 h *in vacuo* and preserved for at least 24 h in a vacuumized desiccator. When releasing the vacuum, nitrogen gas was substituted to protect the spin probe from chemical degradation. The thin film was swollen at 50–60°C by 1/15 M phosphate buffer of adequate pH. The pH of resulting turbid solutions was measured after preparation.

ESR spectra were recorded on a JEOL JES-RE1X spectrometer equipped with a variable temperature controller JEOL ES-DVT2. The spectrometer was operated at centerfield 328.5 mT, scan width ±5 mT, and scan speed 10 mT/4 min. The X band microwave frequency was 9.23 GHz at microwave power 5 mW, the modulation amplitude was 0.5 mT, and the response time (time constant) was 0.1 s. A rectangular ESR cell was used.

Gel Filtration

The thin film of C_nSA without spin-labeled reagent was prepared by a method described above and was swollen by 1/15 M phosphate buffer including 1 mM of water-soluble anionic dye (bromophenol blue). The resulting turbid solutions were sonicated at room temperature for $C_{12}SA$ and $C_{14}SA$ and at 50–60°C for $C_{16}SA$.

After being kept for 2 h at the desired temperature, about 0.5 cm^3 of a solution was eluted with elution medium at the velocity of 3.2 cm^3 min^{-1} on a column (1.6 cm $\phi \times$ 18 cm; Sephadex G-50 gel, medium grade) at-

tached to the water jacket of the desired temperature. The elution medium is 1/15 *M* phosphate buffer at a pH identical to the turbid solution of C_nSA. Before the elution, it was degassed and kept at the desired temperature.

The elution was monitored by optical density at 590 nm, which is an absorption band peak of bromophenol blue. The optical density was measured on JASCO UV/V UVIDEC-340 and Shimadzu UV/V 200S optical photometers using a flow cell.

RESULTS AND DISCUSSION

Phase Transition

Figure 1 shows the DTA charts for a turbid solution of C_{16}SA of 10^{-2} g cm^{-3} at pH 3.49 in 1/15 *M* phosphate buffer. A broad, endothermic peak was observed at 53–70°C on the first heating process (a), a sharp, exothermic peak was detected at 38°C on cooling (b), and a sharp, endothermic peak was observable at 38°C on the second heating (c). Though the cooling and heating processes were repeated afterward, only a peak at 38°C was always observed. With the phase transition on the first heating process, precipitates melted and a resulting turbid solution was maintained even at the subsequent phase transitions.

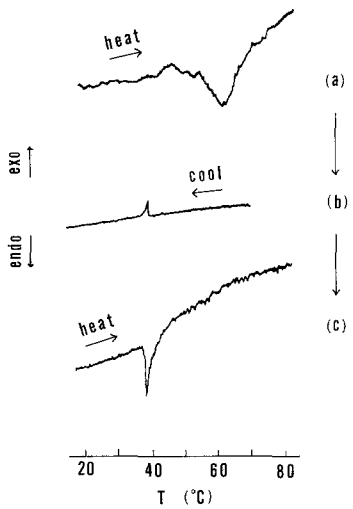

FIG. 1. DTA charts for a turbid solution of C_{16}SA of 10^{-2} g cm^{-3} at pH 3.49 in 1/15 *M* phosphate buffer. (a) heating →, (b) cooling →, (c) heating.

Although the phase transition temperatures were measured for C_{16}SA in water at concentrations between 10^{-2}–10^{-1} g cm^{-3}, two kinds of phase transition temperatures were independent of concentration and almost coincided with those in phosphate buffer.

As well as double-chain amphiphiles (11, 12), recent DSC investigation of aqueous solutions of single-chain amphiphile, C_{16}SA, provided two phase transitions: the higher coagel–liquid crystal transition and the lower metagel–liquid crystal (gel–liquid crystal) transition (6). Two kinds of phase transitions for C_{16}SA vesicle solutions observed in the present work by DTA are in agreement with those in previous work.

The DTA for C_{14}SA at pH 3.48 in 1/15 *M* phosphate buffer revealed a broad, endothermic peak at 45°C on the first heating, a sharp, exothermic peak at 13°C on cooling, and a sharp, endothermic peak at 13°C on the second heating. For C_{12}SA at pH 3.44, a broad peak at 37°C was observed only on the first heating.

The phase transition temperatures of C_nSA of 10^{-2} g cm^{-3} in 1/15 *M* phosphate buffer are plotted as a function of hydrocarbon chain length in Fig. 2. Those increased with the chain length. It can be assumed from the gap between the metagel–liquid crystal phase transition temperatures for C_{14}SA and C_{16}SA that the metagel–liquid crystal phase transition temperature of C_{12}SA vesicle solutions may be below the freezing point of the solutions, which is too low to be measured.

Taking account of experimental results in this and previous works (10), the energy diagram is schematically drawn for C_{16}SA vesicle solutions in Fig. 3, where Gibbs free energy *G* is plotted against temperature *T*. On the first heating process, coagel phase is transformed into liquid crystal phase through the transition temperature at 53°C. On the cooling process, the liquid crystal phase is not transformed into coagel phase but is supercooled at the liquid crystal state. On further cooling, the super-

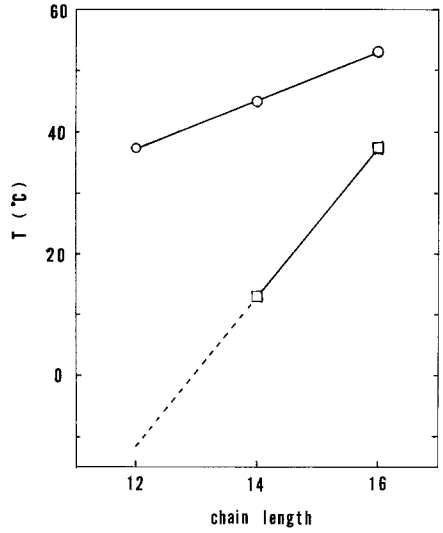

FIG. 2. Phase transition temperatures for turbid solutions of C_nSA of 10^{-2} g cm^{-3} in 1/15 *M* phosphate buffer. (○) coagel–liquid crystal phase transition, (□) metagel–liquid crystal phase transition. $C_{12}SA$, pH 3.44; $C_{14}SA$, pH 3.48; $C_{16}SA$, pH 3.49.

cooled liquid crystal phase is transformed into the metagel phase at 38°C. Similar interpretation can be applied to $C_{12}SA$ and $C_{14}SA$ vesicle solutions. This means that vesicles are in the metastable state at temperatures below coagel–liquid crystal phase transition and may be transformed into the stable coagel state after long periods. This is consistent with the fact that C_nSA vesicle solutions at room temperature (~25°C) precipitate at long periods.

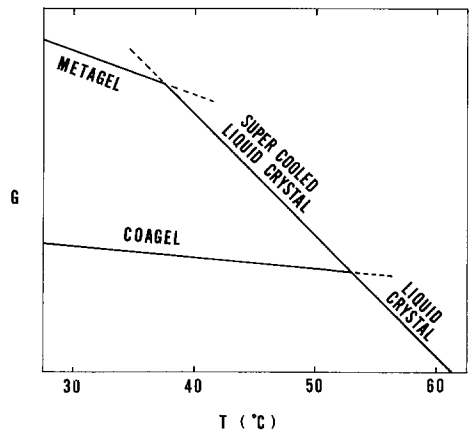

FIG. 3 A. schematic diagram of Gibbs free energy vs temperature for a $C_{16}SA$ vesicle solution of 10^{-2} g cm^{-3} at pH 3.49 in 1/15 *M* phosphate buffer.

Order Parameter

Figure 4 illustrates ESR spectra at various temperatures for a turbid solution of $C_{14}SA$ of 0.5×10^{-2} g cm^{-3} at pH 5.50 in 1/15 *M* phosphate buffer, which includes 7-DOXYL stearic acid of 1 mol%. The line shape of ESR spectra broadens at lower temperatures.

The order parameter S, which is a measure of the distribution of molecular orientations relative to some reference axis, can be evaluated from ESR spectra of *n*-DOXYL stearic acid by using an equation (13, 14):

$$S = (T_{\parallel} - T_{\perp})/[T_{zz} - (T_{xx} + T_{yy})/2]. \quad [1]$$

The parallel and perpendicular hyperfine splitting values for a nitroxide radical, $T_{\parallel}$ and $T_{\perp}$, respectively, are determined from ESR spectra, as illustrated in Fig. 4. T_{xx}, T_{yy}, and T_{zz} are the principal values of hyperfine splitting tensor, and the numerical values are ob-

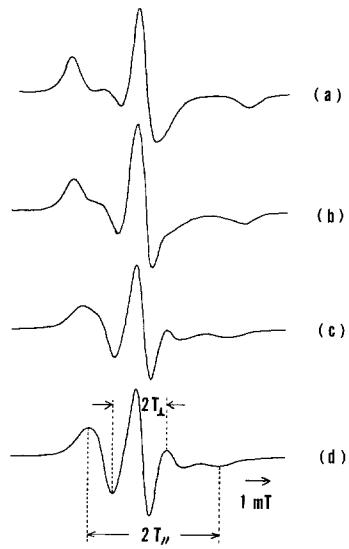

FIG. 4. ESR spectra at various temperatures for a turbid solution of $C_{14}SA$ of 0.5×10^{-2} g cm^{-3} at pH 5.50 in 1/15 *M* phosphate buffer including 7-DOXYL stearic acid of 1 mol%. (a) 2°C, (b) 12°C, (c) 17°C, (d) 25°C.

tained as 0.63, 0.58, and 3.36 mT, respectively, for a single crystal of 5-DOXYL stearic acid (15). Those were also applied to all n-DOXYL stearic acids.

The $T_\perp$ value can not be always determined directly from ESR spectra when the positive band at high field is not clarified, as seen in spectra at lower temperatures in Fig. 4. Then the order parameter is able to be evaluated by

$$S = 3(T_{\parallel} - a_N)/[2T_{zz} - (T_{xx} + T_{yy})] \quad [2]$$

and

$$a_N = (T_{xx} + T_{yy} + T_{zz})/3 \approx (T_{\parallel} + 2T_\perp)/3, \quad [3]$$

where a_N is the isotropic splitting constant.

Figure 5 shows order parameters of 7-DOXYL stearic acid in turbid solutions of C_nSA as a function of temperature. The order parameters were evaluated by the use of Eq. [2]. Those were in good agreement with the numerical value obtained on the basis of Eq. [1] from the spectra in which the $T_\perp$ values can be determined. The order parameters decrease with increases in temperature for all C_nSA: While those in C_{12}SA solutions monotonously decrease with the temperature, those in C_{14}SA and C_{16}SA solutions cooperatively decrease by about 15 and 35°C, respectively.

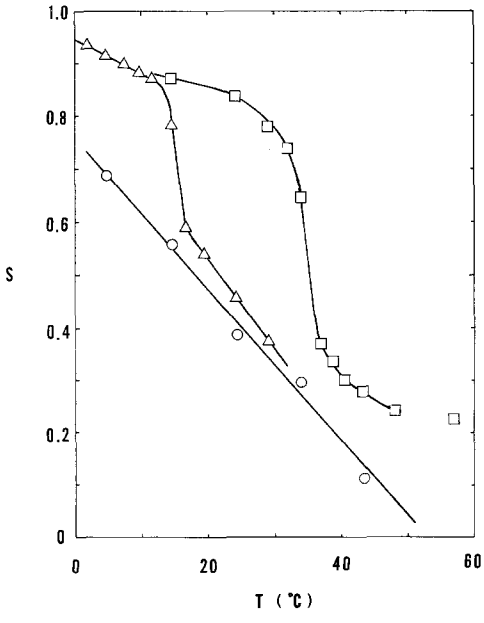

FIG. 5. Order parameters as a function of temperature for 7-DOXYL stearic acid included in turbid solutions of C_nSA of 0.5×10^{-2} g cm^{-3} in 1/15 M phosphate buffer. (○) C_{12}SA (pH 5.37), (△) C_{14}SA (pH 5.50), (□) C_{16}SA (pH 5.56).

The trans–gauche configurational change on hydrocarbon chains of amphiphiles occurs with the metagel–liquid crystal phase transition, and the order structure of hydrophobic moiety is disorganized in the liquid crystal state. Such variation is observed from the temperature dependence of ESR spectra for vesicle solutions including a spin probe and n-DOXYL stearic acid: the local environment near the N-oxyloxazolidine ring of n-DOXYL stearic acid is reflected on the hyperfine splitting of ESR spectra. Therefore, the temperature dependence of the order parameter of n-DOXYL stearic acid reflects the change of the degree of order of the vesicle membrane followed by the metagel–liquid crystal phase transition.

The cooperative decrease of the order parameter at a certain temperature for C_{14}SA and C_{16}SA vesicle solutions indicates that the order structure of vesicle membranes around spin probes changes remarkably around this temperature and the fluidity of the membranes increases. The transition temperatures of the order parameter are in agreement with those of metagel–liquid crystal on DTA charts. On the other hand, the order parameter for C_{12}SA vesicle solutions decreases linearly at 5–45°C, at which there is no metagel–liquid crystal phase transition.

Figure 6 shows the logarithmic values of order parameters of n-DOXYL stearic acids (n = 5, 7, 12, 16) in turbid solutions of C_{14}SA as a function of the location of N-oxyloxazolidine ring, k ($= n - 2$). These values decrease with increasing k: the closer the N-oxyloxazolidine ring is to the terminal methyl group, the smaller the order parameter is.

The order structure is not always uniform at the inside of a bilayer membrane. Carboxyl

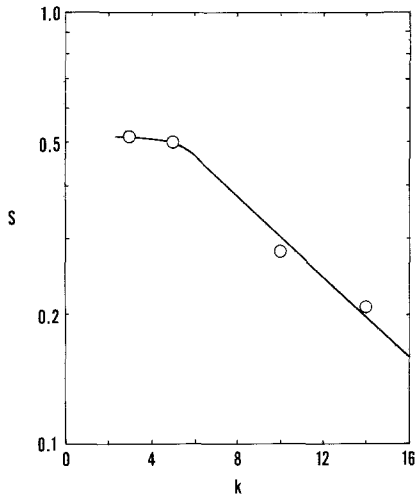

FIG. 6. Order parameters at room temperature as a function of the position of *N*-oxyloxazolidine ring in *n*-DOXYL stearic acid included in turbid solutions of $C_{14}SA$ of 0.5×10^{-2} g cm^{-3} at pH 5.56 in 1/15 *M* phosphate buffer.

moiety of *n*-DOXYL stearic acids locates on the membrane surface, and their hydrocarbon moiety orients almost normal to it (5). Therefore, some *n*-DOXYL stearic acids that attach *N*-oxyloxazolidine rings to different positions on their hydrocarbon chains are utilized to examine the fluidity gradient of amphiphile hydrocarbons from the membrane surface to the membrane center (5, 13, 16). It can be recognized for $C_{14}SA$ vesicles at room temperature that the interior of the membrane tends to be more flexible in the order structure than the exterior of the membrane does.

ESR of smectic liquid crystal of sodium decanoate–decanol–water mixture as a model of bilayer membranes was investigated using *n*-DOXYL stearic acid (14). The logarithmic order parameter changed linearly with the location of the *N*-oxyloxazolidine ring. Such a relation was possible if a hydrocarbon chain in smectic liquid crystal was approximated by a Porod–Kratcky model.

Smith *et al.* (17–19) have measured deuterium–NMR and spin probe ESR of deuterium- and nitroxide-labeled phospholipids and examined the fluidity gradient in lipid bilayers from the order parameters. The absolute values of order parameters from spin probe ESR were lower than those from deuterium NMR, because bilayer membranes were perturbed due to the bulky nature of nitroxide moiety of spin probe. On the other hand, they demonstrated that, while the order parameters from deuterium NMR decreased with the position from the carboxy terminal of labeled carbon in stearic acid, they were constant at the close positions from the carboxy terminal. This was explained as the higher probability of "kinks" (gauche–trans–gauche conformer combinations) at a hydrocarbon chain position near the carboxy terminal.

On the plot of order parameter vs location of *N*-oxyloxazolidine ring in *n*-DOXYL stearic acid, the log *S* values for $C_{14}SA$ vesicle solutions have a linear relation to the *k* values above 5. This may mean that the hydrocarbon chain of C_nSA behaves like a Porod–Kratcky chain. On the other hand, the deviation at $k = 3$ from a straight line on a log *S* vs *k* plot can be interpreted as a result of the *N*-oxyloxyazolidine ring of 5-DOXYL stearic acid ($k = 3$) approaching to trans ethylene moiety of $C_{14}SA$ rather than of the occurrence of kinks.

Trapping Efficiency

The solid and broken lines in Fig. 7 are elution patterns of bromophenol blue at 25 and 50°C, respectively, for sonicated solutions of

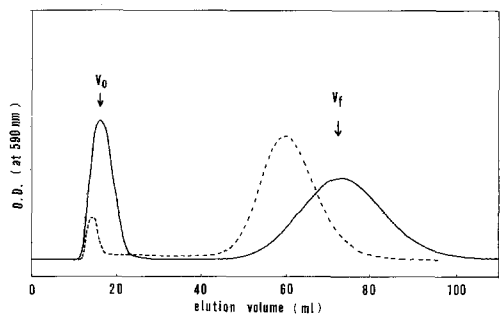

FIG. 7. Elution patterns for sonicated solutions of $C_{16}SA$ of 0.5×10^{-2} g cm^{-3} at pH 5.39 in 1/15 *M* phosphate buffer prepared with bromophenol blue. (—) 25°C, (---) 50°C.

$C_{16}SA$ of 0.5×10^{-2} g cm^{-3} at pH 5.39 in 1/15 M phosphate buffer. There are two peaks of the void volume V_o and free dye volume V_f on elution patterns. The V_o peak at 50°C is smaller than that at 25°C, indicating the less trapping of dye. The slight elution of dyes was observed at the elution volumes between V_o and V_f peaks at 50°C. This is consistent with the following fact: on the elution through Sephadex gel in a column at 50°C, blue colors ran from the blue band of bromophenol blue trapped in the $C_{16}SA$ vesicles.

The fractions of V_o and V_f were collected, and the trapping efficiency was calculated at various temperatures as follows:

$$\text{trapping efficiency (\%)} = \frac{\text{trapped dyes}}{\text{total dyes}} \times 100. \quad [4]$$

The trapping efficiency is plotted as a function of the elution temperature in Fig. 8. It remarkably decreases beyond 35°C. The same procedure was carried out at 25°C for the turbid solutions of $C_{16}SA$ of 0.5×10^{-2} g cm^{-3} at various pH. The trapping efficiency was independent of pH 5.39 to 6.06.

The membrane fluidity differs fairly between gel and liquid crystal phases, and the membrane permeation kinetics is considerably largely influenced by it. Successively, the membrane permeability affects the trapping efficiency of the solutes in the inner aqueous phases of vesicles, which can be estimated from the gel filtration. The permeability coefficients of Cresol red (*o*-cresolsulfonphthalein) entrapped in the inner aqueous phases of dimyristoylphosphatidic acid vesicles were compared between gel and liquid crystal phases (20). The Cresol red leakage was almost null even after 4 h in gel phase but was 50% after 50 min in liquid crystal phase.

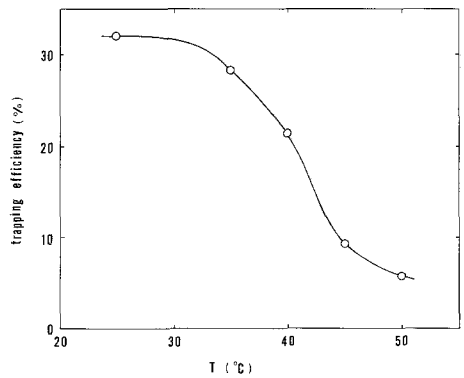

FIG. 8. Temperature dependence of the trapping efficiency for sonicated solutions of $C_{16}SA$ of 0.5×10^{-2} g cm^{-3} at pH 5.39 in 1/15 M phosphate buffer prepared with bromophenol blue.

On the gel filtration of C_nSA vesicle solutions, when the vesicles separated from free dyes in bulk at the top of column pass through Sephadex G-50 gel in a column, the osmotic pressure difference occurs in and out of vesicle membrane. Then bromophenol blue in vesicles percolates the membrane depending on the membrane fluidity at each temperature. Therefore, the trapping efficiency is a measure of the percolation velocity or membrane percolation, and in fact the trapping efficiency of $C_{16}SA$ vesicles depends on the temperature as seen in Fig. 8.

Table 1 lists the trapping efficiency at 25°C for a sonicated solution of $C_{12}SA$ at pH 5.56 and at 1.5 and 25°C for sonicated solutions of $C_{14}SA$ at pH 5.42 and compares them with the values for sonicated solutions of $C_{16}SA$ at various temperatures. The trapping efficiency at 25°C for $C_{12}SA$ and $C_{14}SA$ is nearly null, but that at 1.5°C for $C_{14}SA$ is significant. The trapping efficiency for $C_{16}SA$ is larger than those for $C_{14}SA$ and $C_{12}SA$.

The trapping efficiency of $C_{16}SA$ vesicles decreases at 35–40°C where the metagel–liquid crystal phase transition occurs. It can be suggested that bromophenol blue is percolated through the vesicle membrane from inner aqueous phases in vesicles at the temperatures above the phase transition, that is, in liquid crystal state. $C_{12}SA$ and $C_{14}SA$ vesicles are in liquid crystal state at room temperature, which is higher than the metagel–liquid crystal phase transition temperature, and the trapping efficiency is null for both $C_{12}SA$ and $C_{14}SA$ vesicles, indicating the very high permeability of membrane. However, the trapping efficiency

TABLE I

Trapping Efficiency for C_nSA Vesicle Solutions of 0.5×10^{-2} g cm^{-3}

C_nSA type	pH	Elution temperature (°C)	Trapping efficiency (%)
$C_{12}SA$	5.56	25	~0
$C_{14}SA$	5.42	1.5	24.2
		25	~0
$C_{16}SA$	5.39	25	32.1
		35	28.4
		40	21.5
		45	9.4
		50	5.8

of $C_{14}SA$ vesicles fairly increases at 1.5°C, which is lower than the metagel–liquid crystal phase transition temperature, and the membrane permeability is depressed more remarkably than that at room temperature.

CONCLUDING REMARKS

The characterization has been carried out for C_nSA vesicles in aqueous media. The vesicles formed by single-chain amphiphiles, C_nSA, was similar to double-chain amphiphilic vesicles in many respects.

(1) The C_nSA solutions undergo a thermal phase transition. Those present coagel–liquid crystal and metagel–liquid crystal phase transitions. The transition temperatures increase with increasing hydrocarbon chain length.

(2) The order parameters for C_nSA cooperatively decrease around the metagel–liquid crystal transition temperature. It is suggested that the order structure of vesicle membranes is remarkably different in two phases.

(3) The order structure is not always uniform at the inside of a bilayer membrane, but the interior of the vesicle membrane is more fluid than the exterior of the membrane.

(4) The existence of the inner aqueous phases of vesicles has been confirmed by the significant trapping efficiency of the solutes. The trapping efficiency decreases at metagel–liquid crystal phase transition temperature. This means that the motional state of vesicle membrane is less restricted in the liquid crystal and the membrane permeability is higher.

ACKNOWLEDGMENTS

We are grateful to Professors R. Ikeda and O. Yamauchi, Nagoya University, for their generous permission to use DTA and ESR instruments and for the technical assistance of their coworkers.

REFERENCES

1. Hinz, H.-J., and Sturtevant, J. M., *J. Biol. Chem.* **247,** 6071 (1972).
2. Chapman, D., *Quart. Rev. Biophys.* **8,** 185 (1975).
3. Linden, C. D., Wright, K. L., McConnel, H. M., and Fox, C. F., *Proc. Nat. Acad. Sci. USA* **70,** 2271 (1973).
4. Shinitzky, M., and Barenholz, Y., *Biochim. Biophys. Acta* **515,** 367 (1978).
5. Hubbell, W. L., and McConnell, H. M., *J. Amer. Chem. Soc.* **93,** 314 (1971).
6. Satoh, N., and Tsujii, K., *J. Phys. Chem.* **91,** 6629 (1987).
7. Imae, T., and Trend, B., *J. Colloid Interface Sci.* **145,** 207 (1991).
8. Imae, T., and Trend, B., *Langmuir* **7,** 643 (1991).
9. Nakazawa, K., Imae, T., and Iwamoto, T., submitted for publication.
10. Imae, T., Suzuki, S., Abe, A., Ikeda, S., Fukui, Y., Senoh, M., and Tsujii, K., *Colloids Surf.* **33,** 75 (1988).
11. Kodama, M., Kuwabara, M., and Seki, S., *Biochim. Biophys. Acta* **689,** 567 (1982).
12. Kodama, M., Kunitake, T., and Seki, S., *J. Phys. Chem.* **94,** 1550 (1990).
13. Schreier, S., Polnaszek, C. F., and Smith, I. C. P., *Biochim. Biophys. Acta* **515,** 375 (1978).
14. Seeling, J., *J. Amer. Chem. Soc.* **92,** 3881 (1970).
15. Jost, P. C., and Griffith, O. H., *in* "Methods in Enzymology" (C. S. W. Hirs and S. N. Timasheff, Eds.), Vol. 49, p. 369, Academic Press, San Diego, 1978.
16. Jost, P., Libertini, L. J., Hebert, V. C., and Griffith, O. H., *J. Mol. Biol.* **59,** 77 (1971).
17. Stockton, G. W., Polnaszek, C. F., Tulloch, A. P., Hasan, F., and Smith, I. C. P., *Biochemistry* **15,** 954 (1976).
18. Smith, I. C. P., Stockton, G. W., Tulloch, A. P., Polnaszek, C. F., and Johnson, K. G., *J. Colloid Interface Sci.* **58,** 439 (1977).
19. Smith, I. C. P., Tulloch, A. P., Stockton, G. W., Schreier, S., Joyce, A., Butler, K. W., Boulanger, Y., Blackwell, B., and Bennett, L. G., *Ann. N.Y. Acad. Sci.* **308,** 8 (1978).
20. Elamrani, K., and Blume, A., *Biochim. Biophys. Acta* **727,** 22 (1983).